An integrated approach for the analysis and modeling of road tunnel ventilation. Part II: Numerical model and its calibration

P. Cingi [a], D. Angeli [a,b,*], M. Cavazzuti [b,c], P. Levoni [b], E. Stalio [c], M. Cipollone [d]

[a] DISMI, Dipartimento di Scienze e Metodi dell'Ingegneria, Università degli Studi di Modena e Reggio Emilia, Via Amendola 2, Reggio Emilia 42122, Italy
[b] Mimesis srl, via Contrada 309, Modena 41126, Italy
[c] DIEF, Dipartimento di Ingegneria "Enzo Ferrari", Università degli Studi di Modena e Reggio Emilia, Via Vivarelli 10, Modena 41125, Italy
[d] GEIE-TMB – Gruppo Europeo di Interesse Economico del Traforo del Monte Bianco, Piazzale Sud del Traforo del Monte Bianco, Courmayeur, AO 11013, Italy

ARTICLE INFO

ABSTRACT

The present work represents the second and final part of a twofold study aiming at the definition and validation of an integrated methodology for the analysis and modeling of road tunnel ventilation systems. A numerical approach is presented, based on the Finite Volume integration of the 1D mechanical and thermal energy conservation equations on a network of ducts, representing the ventilation system of the 11.6 km long Mont Blanc Tunnel. The set of distributed and concentrated loss coefficients, representing dissipation of mechanical energy by friction in each part of the ventilation system, is calibrated against a rich experimental dataset, collected throughout a dedicated set of in situ tests and presented in the first part of the work. The calibration of the model is carried out by means of genetic optimization algorithms. Predictions of the flow field using the calibrated parameters are in remarkable agreement with the experimental data, with an overall RMS error of $\pm$ 0.27 m/s, i.e. of the same order of the accuracy of the measurement probes. Further validation against a selection of field data recorded by the tunnel monitoring and control system is brought forward, highlighting the robustness and potential general applicability of the proposed approach.

1. Introduction

In many civil infrastructures, including road and railway tunnels, underground stations and car parks, ventilation control is crucial for the safety of users. This is even more the case when operating in emergency conditions, since air velocity is one of the main factors influencing smoke or pollutants distribution in case of fire or other hazardous events. Therefore, the availability of a fast and reliable model capable of predicting ventilation flows in such systems is of great importance for the design and rapid testing of airflow control strategies, aimed at quickly containing and evacuating vitiated air from the areas occupied by users.

As stated in Part I of this work [1], a series of studies concerning the Mont Blanc Tunnel (TMB) ventilation system were undertaken in the framework of an extensive collaboration among the institutions and companies involved in the present, twofold endeavour. These studies, whose results have all been pivotal to the development of the computational model presented here, employed different approaches, including multi-point in situ velocity measurements with fixed-point anemometers [2,3], simplified semi-analytical models [4] and CFD analyses concerning local effects of axial fans [5], with the aim of gathering as much information as possible on the fluid dynamic characteristics of the TMB ventilation system.

In this second part of work, a computational tool is presented, specifically developed to predicting the airflow distribution in the TMB ventilation system. The choice of developing an in-house tool, instead of resorting to commercial 1D network flow solvers or general-purpose scientific computation packages, is motivated by a number of inherent advantages, including the high degree of customization, ease of portability and deployment, and code reuse, for example in a co-simulation (also known as multi-scale) framework.

Examples of a variety of different approaches for the numerical modeling of airflow in road tunnels can be found in the literature. The earliest attempts consisted in 1D models based on the Hardy-Cross methods: notable examples can be found in [6,7]. Despite its relative simplicity, such an approach is still considered as a convenient option [8]. A slightly different, one-dimensional approach for the simulation of duct networks is presented in [9] where generic network is modeled as a directed graph. Mass, energy and species conservation equations are solved at the nodes while the momentum conservation equations are solved along branches.

* Corresponding author at: DISMI, Dipartimento di Scienze e Metodi dell'Ingegneria, Università degli Studi di Modena e Reggio Emilia, Via Amendola 2, 42122 Reggio Emilia, Italy.
E-mail address: diego.angeli@unimore.it (D. Angeli).

Nomenclature

A	incidence matrix [–]
A	cross section [m^2]
c	specific heat [J kg^{-1} K^{-1}]
D_h	hydraulic diameter [m]
f	friction factor [–]
g	gravitational acceleration [m s^{-2}]
k_E, m_E	thermal power source term coefficients [W m^{-3}, W m^{-3} K^{-1}]
k_M, m_M	mechanical energy source term coefficients [J m^{-3}, J s m^{-4},]
L	length [m]
P	total pressure [Pa]
q_g	generated thermal power per unit volume [W m^{-3}]
R	gas constant [J kg^{-1} K^{-1}]
s	longitudinal coordinate [m]
T	temperature [ºC]
u	velocity [m s^{-1}]
U	heat transfer coefficient [W m^{-2} K^{-1}]
w	mean longitudinal velocity [m s^{-1}]
x	longitudinal coordinate [m]
y	wall-normal coordinate [m]

Greek symbols

β	concentrated loss coefficient [–]
$\gamma_{0,1,2}$	fan curves coefficients [J s^{0,1,2} m s-3,-4,-5 –]
ρ	density [kg m^{-3}]
σ_M	volumetric mechanical energy source term [J m^{-3}]
σ_E	volumetric thermal power source term [W m^{-3}]
ω	upwinding operator [–]

Superscripts

$\cdot$	flow rate
$^-$	boundary value
$*$	initial guess
$\prime$	correction

Subscripts

bn	branch-to-node
fan	fan
i	node index
j	branch index
l	auxiliary index
$loss$	friction loss
nb	node-to-branch

More recently, attempts at full scale 3D modeling were presented [10,11], their feasibility being largely due to the increase in computational resources with respect to previous decades. On the other hand the advantages offered by simplified models are proven to be still alluring, given the variety of relatively recent studies employing 0D or 1D models [4,12].

An interesting compromise between these two extremes has been proposed by Colella et al. through the design of multiscale (or co-simulation) models which combine a lean, simple network model with local use of 3D CFD for the accurate modeling of relevant flow details [13–15]. More recently Vermesi et al. [16] provided a proof of the computational advantage guaranteed by the usage of multiscale models. The case study was solved employing FDS for one third of the domain, including the fire, and a 1D graph representation for the remaining part; then a full scale, parallel 3D simulation was performed using Ansys Fluent. The difference between the resulting temperature fields were limited to 2%, with a computational time saving as high as 97%.

Field data are rarely employed in numerical studies on road tunnels, due to the difficulty of performing in situ measurements. When

such data is available, it is most commonly used for the validation of a model than for its calibration [17]. Nonetheless, few examples of model calibration based on full scale experimental data can be found in the literature. For instance, Jang and Chen employed a 1D model for determining, through and optimization process, the aerodynamic coefficients of highway tunnels [18].

In light of the aims of the present research, the choice of the numerical approach fell on a 1D model, based on an oriented graph. The development of such model has been carried out under an object-oriented logic, thus making the resulting numerical code customizable and thus potentially adaptable to problems of the same kind. The resulting numerical procedure is described in detail in Section 2 of the present paper.

In the numerical model, all the relevant thermo-fluid dynamic features of the Mont Blanc Tunnel ventilation system are modeled by means of integral transfer parameters. Such parameters need to be finely tuned based on reliable physical data, in order for the model to reproduce the the behavior of the actual system with satisfactory accuracy. For this reason, the experimental data set collected by means of a continuous airflow acquisition facility and described in the first part of the present work [1] was used as reference for the calibration of these parameters, performed by means of a genetic optimization algorithm, outlined in Section 3.

A comparison between model prediction and calibration data is brought forth in Section 4. The calibrated model is then employed to provide further validation against a selection of field velocity data recorded by the tunnel monitoring and control system under extremely diverse environmental boundary conditions. Such data set, despite being less rich and accurate than the continuous airflow acquisition measurements carried out for the calibration, represents nevertheless a good benchmark, since it is indeed completely independent from the calibration data.

Despite its lower accuracy with respect to 3D full scale models, the present method is proven to be a convenient and lightweight computational tool, capable of reproducing different ventilation scenarios potentially occurring in the Mont Blanc Tunnel with satisfactory accuracy, and applicable with relative ease to a large variety of similar systems.

2. Numerical method

2.1. Governing equations

Detail of the physical system considered as case study, i.e. the Mont Blanc Tunnel ventilation system, are reported in Part I of the present study [1] and are not repeated here for the sake of brevity. Airflow in the main tunnel and ventilation channels can be modeled by solving a system of differential equations expressing conservation of mass, mechanical energy and thermal energy, under the following assumptions:

- as the air velocity in the tunnel is proven to be significantly lower than the speed of sound, the flow can be considered incompressible;
- however, in such systems, density variations as a function of temperature are typically not negligible [4]; hence, air density is determined by means of an incompressible ideal gas law, where pressure is fixed at a suitable reference value; this, in principle, would imply the presence of a compression work term in the mechanical energy balance, which, however, is considered as negligible;
- steady-state conditions are considered only (although the proposed approach can be extended to time-dependent problems rather effortlessly);
- since the physical system is characterized by a very high aspect ratio, all the variables can be considered as dependent from a single spatial coordinate, which will be from now on called x;
- the term representing viscous dissipation in the mechanical energy balance equation is expressed by a loss term σ_{loss} depending only on velocity u;
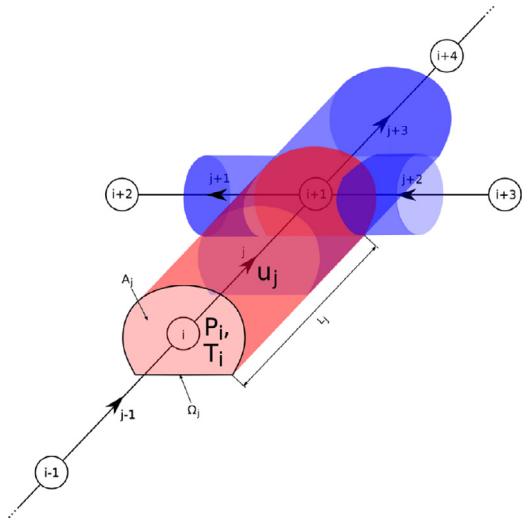
Fig. 1. Control volumes associated to branches (red) and nodes (blue).

- likewise, mechanical energy sources such as fans can be represented by a source term σ_{fan};
- the diffusive term of the thermal energy equation along x is assumed as irrelevant with respect to the convective term and can be omitted; viscous dissipation is also neglected in the thermal energy equation, while wall heat transfer and internal heat generation are expressed by the source term σ_E.

A trotal pressure P is defined, allowing for a more compact representation of mechanical energy conservation:

$$P = \frac{\rho u^2}{2} + p + \rho \ g(z - z_0) \tag{1}$$

In light of the above assumptions, the governing equations can be written in the following form:

$$\begin{cases} \frac{d(\rho u)}{dx} = 0 \\ \frac{dP}{dx} = \frac{d}{dx}\left(-\sigma_{M,loss} + \sigma_{M,fan}\right) \\ \rho c u \frac{dT}{dx} = \sigma_E \\ \rho = \frac{p_{ref}}{RT} \end{cases} \tag{2}$$

2.2. Topological representation

The network of ducts and channels constituting the typical ventilation system of a tunnel can be conveniently represented by a directed graph. Such a graph also constitutes the support for Finite Volume discretization of Eq. (2). The system is subdivided into control volumes coinciding with the branches of the directed graph. Each branch, in turn, is connected to two nodes. Contrarily to branches nodes are not characterized by a volume nor a mass per se, but merely represent interfaces of zero volume among concurrent branches. However, in a Finite Volume framework, a staggered mesh can be defined such that the domain associated to the ith node is composed by half of all branches attached to the jth node (see Fig. 1). The connectivity between nodes and branches is expressed by the incidence matrix $\mathbf{A}$ of the graph, see [19] for details.

It is then possible to define different variables to node and branch domains. State variables such as temperature, total (or static) pressure, density, specific heat are defined on nodes; flow variables (mass flow rates and thus velocities) are defined on branches. Each branches also possesses specific geometric, thermodynamic and fluid-dynamic properties (length, section area, wall temperature, mechanical sinks and sources, heat transfer coefficients).

2.3. Discrete equations

The discrete form of Eqs. (1) and (2), applied on the graph representation of the system, reads:

$$\sum_j a_{ij} A_j \rho_j u_j = 0 \tag{3}$$

$$\sum_i a_{ij} P_i + \left(\sigma_{M,fan,j} - \sigma_{M,loss,j}\right) = 0 \tag{4}$$

$$\sum_j a_{ij} \rho_j c_j A_j u_j T_j = \sigma_{E,i} \tag{5}$$

The index i (j) indicates that the indexed variable refers to a node (branch), and a_{ij} is the corresponding element of the incidence matrix. Eqs. (3) and (5) are written on the staggered subdivision for unknowns that are defined on nodes, while Eq. (4) is written for the unknown u, which is defined on branches. Friction losses, along with mechanical and thermal energy source terms, can be defined as follows:

$$\sigma_{M,loss,j} = \left(\frac{f_j L_j}{D_{h,j}} + \beta_j\right) \frac{\rho_j u_j |u_j|}{2} \tag{6}$$

$$\sigma_{M,fan,j} = \gamma_0 + \gamma_1 u_j + \gamma_2 u_j^2 \tag{7}$$

$$\sigma_{E,j} = \frac{4U_j}{D_{h,j}}\left(T_j - T_w\right) + q_{g,j} \tag{8}$$

It is important to point out that the expression of quantities defined on nodes in terms of their values on branches, and vice-versa, is done by means of upwind operators. The operator ω_{nb} is defined for node-to-branch upwinding:

$$\omega_{nb,ij} = \frac{1}{2} \sum_i \left(|a_{ij}| + a_{ij} \frac{u_j}{|u_j|}\right) \tag{9}$$

such that, for instance, $\rho_j = \sum_i \omega_{nb,ij} \rho_i$. Similarly, an operator ω_{bn} can be defined for branch-to-node upwinding:

$$\omega_{bn,ij} = \frac{1}{2} \sum_j \left(|a_{ij}| - a_{ij} \frac{u_j}{|u_j|}\right) \tag{10}$$

such that, e.g., $\sigma_{E,i} = \sum_j \omega_{bn,ij} \sigma_{E,j}$

The source and sink terms described by Eqs. (6) and (7), which are defined on branches and have a nonlinear dependence on local velocity, have been linearized to the form of $\sigma = m_M u + k_M$. Within the iterative solution loop described in the following paragraphs, velocity at a given iteration k is used to incorporate nonlinear terms in the coefficient m for the subsequent iteration $k + 1$, e.g.:

$$m_{M,j,loss,k+1} = \rho_j \left(\frac{f_j L_j}{D_{h,j}} + \beta_j\right) \frac{|u_{j,k}|}{2} \tag{11}$$

In a similar fashion, the thermal energy source terms $\sigma_{E,j}$, can be decomposed in the form $\sigma_{E,j} = m_{E,j} T_j + k_{E,j}$.

The discrete governing equations can be conveniently recast in matrix form. Mass conservation (Eq. (3)) becomes:

$$(\mathbf{A}\,\mathbf{M} - \mathbf{E})\mathbf{u} = \mathbf{0} \tag{12}$$

Where $\mathbf{u}$ is the branches velocity vector, of length n_b. $\mathbf{M}$ is a diagonal matrix $n_b \times n_b$ of elements:

$$\mu_{jj} = A_j \rho_{j,n+1} \tag{13}$$

The elements of $n_n \times n_n$ $\mathbf{E}$, functional to the correct processing of boundary nodes, are defined as follows:

$$e_{ij} = \begin{cases} -\sum_l a_{il} \mu_{lj} & \forall i \in I_b \\ 0 & \forall i \notin I_b \end{cases} \tag{14}$$

Mechanical energy conservation (Eq. (4)) may be expressed as:

$$\mathbf{A}^T \mathbf{p} = \mathbf{Y} \mathbf{u} + \mathbf{k} \tag{15}$$

where $\mathbf{p}$ is the vector containing nodal total pressure values, of length n_n, $\mathbf{Y}$ is a diagonal matrix $n_b \times n_b$ of elements:

$$y_{jj} = m_{M,fan,j} + m_{M,loss,j} \tag{16}$$

and $\mathbf{k}$ is an array of elements $k_{M,fan,j}$, one for each branch.

Energy conservation (Eq. (5)) has a simpler form:

$$\mathbf{W} \mathbf{t} = \mathbf{s} \tag{17}$$

where $\mathbf{t}$ is the vector containing nodal temperature values, of length n_n, and the elements of the $n_n \times n_n$ matrix $\mathbf{W}$ are defined as:

$$w_{ij} = \begin{cases} \sum_l \omega_{nb,il} \left(\rho_l c_l A_l u_l a_{lj} + \omega_{nb,lj} m_{E,j} \right) & \forall i \notin I_b \\ 1 & \forall i \in I_b \wedge i = j \\ 0 & \forall i \in I_b \wedge i \neq j \end{cases} \tag{18}$$

Once again special elements are defined for the management of boundary nodes.

The array of known terms $\mathbf{s}$ is made of elements of the form:

$$s_i = \begin{cases} \sum_j \omega_{nb,ij} k_{E,j} & \forall i \notin I_b \\ \frac{1}{2} \sum_j \left[|a_{ij}| \left(\overline{T}_i + T_j \right) + a_{ij} \frac{u_j}{|u_j|} \left(\overline{T}_i - T_j \right) \right] & \forall i \in I_b \end{cases} \tag{19}$$

The above formulation for known terms on boundary nodes implements an inlet-outlet condition for temperature: if the velocity field is such that node i is an inlet, then the boundary value $\overline{T}_i$ is enforced, whereas if flow exits from node i the value T_j is taken from the adjacent branch.

2.4. Solution algorithm

Eqs. (3), (15), and (17) are solved by means of a customized version of the well-known *SIMPLE* algorithm [20], see also [21] for details. Guessed fields ($\mathbf{p}^*$ and $\mathbf{u}^*$) and a variable correction fields ($\mathbf{p}'$ and $\mathbf{u}'$) are defined for pressure and velocity:

$$\mathbf{p} = \mathbf{p}^* + \mathbf{p}' \tag{20}$$

$$\mathbf{u} = \mathbf{u}^* + \mathbf{u}' \tag{21}$$

The iterative procedure starts from the guessed pressure field $\mathbf{p}^*$. By introducing such field in Eq. (15), it is possible to determine the guessed velocity field $\mathbf{u}^*$:

$$\mathbf{u}^* = \mathbf{Y}^{-1} (\mathbf{A}^T \mathbf{p}^* - \mathbf{k}) \tag{22}$$

By introducing definitions (20) into Eq. (15), and subsequently simplifying it using Eq. (22), a correlation between pressure correction $\mathbf{p}'$ and velocity correction $\mathbf{u}'$ can be carried out:

$$\mathbf{u}' = \mathbf{Y}^{-1} \mathbf{A}^T \mathbf{p}' \tag{23}$$

Then, introducing Eqs. (23) and (20) into the continuity equation (13), a linear system is obtained:

$$\mathbf{\Lambda} \mathbf{p}' = \mathbf{b} \tag{24}$$

where the $n_n \times n_n$ matrix $\mathbf{\Lambda}$ is made up by elements of the form:

$$\lambda_{ij} = \begin{cases} \sum_l a_{il} \frac{A_l \rho_l}{m_{loss,l} + m_{fan,l}} a_{lj} & \forall i \notin I_b \\ 1 & \forall i \in I_b \wedge i = j \\ 0 & \forall i \in I_b \wedge i \neq j \end{cases} \tag{25}$$

The known term $\mathbf{b}$ has elements of the form:

$$b_j = \begin{cases} \sum_j a_{ij} A_j \rho_{b,j} u'_j & \forall i \notin I_b \\ 0 & \forall i \in I_b \end{cases} \tag{26}$$

A suitable choice of null and unitary elements within the system [24] allows the application of boundary conditions: the rows referring to boundary nodes are changed to the simple identity $P'_i = 0$.

After each predictor–corrector step of the SIMPLE algorithm, the energy equation is solved with the updated fields, and density is finally updated as a function of the newly obtained node temperature field. The iterative procedure stops when the infinity norm of the pressure correction field $\|\mathbf{p}'\|_\infty$ lies within a specified tolerance.

3. Model calibration

3.1. Choice of calibration parameters

The 1D network representing the Mont Blanc Tunnel ventilation system is composed of 2639 nodes and 3904 branches. As thoroughly described in Part I of the present work [1], as well as in [4], the ventilation system is composed of the tunnel itself, 8 underground fresh air intake (AF) channels and an exhaust air extraction (AV) channel, and a number of inlet and extraction vents connecting the main tunnel with the corresponding channel. For the present model, a spatial resolution of 10 m has been adopted for the tunnel and AF channels, in order to represent each single fresh air inlet vent, while a resolution of 100 m, corresponding to the spacing of exhaust vents, has been kept for the AV channels.

Geometric features (length, section area and perimeter) of the system are known for every branch in the network; so are the characteristic curves of all the fans operating in the tunnel and in ventilation channels. On the other hand, fluid dynamic characteristics such as friction loss coefficients are impossible to measure, at least directly, and thus have to be determined based on reliable physical data. Therefore, the longitudinal velocity profiles presented in Part I of the study [1] have been employed for this task.

The objective of the calibration is the assignment of proper friction factors to each branch of the network. However, the choice of a suitable set of parameters is a crucial issue, as increasing their number exponentially increases the number of tests necessary to obtain a proper sampling of the parameters space. Therefore, the following assumption have been made: (i) a unique friction factor value f_{tunnel} was assigned to all the branches representing the tunnel domain, in line with previous studies [4]; (ii) a different friction factor was defined for each of the 8 AF channels ($\vec{f}_{AF}$) and for the AV channel (f_{AV}), and assigned to the corresponding branches; concentrated loss coefficients were defined for inlet vents (β_{vent}), open exhaust air vents (also called "traps", $\beta_{trap,open}$) and closed exhaust air vents ($\beta_{trap,shut}$), and assigned to all the corresponding branches connecting the ventilation channels to the main tunnel. Hence, the overall number of parameters to be calibrated amounts to 13 loss coefficients.

Some additional observations on the choice of these parameters are in order. First, the definition of a concentrated loss coefficient in place of a friction factor for branches representing vents is due to the irregularity of these ducts, whose path, described in greater detail in [1], presents many bends and section changes, and is better represented by a single loss coefficient. Furthermore, the adoption of a loss coefficient for closed exhaust vents (which apparently sounds paradoxical) is necessary to capture the leakages occurring through these barriers, which were clearly revealed by the measured velocity profile in the last of the five tests performed for this work (see [1]). Lastly, although an estimate of the value of the friction factor of the tunnel, $f_{tunnel} = 0.0235$, had been previously estimated by Levoni et al. [4], such parameter has been added nevertheless to the calibration space, in order to allow more flexibility to the optimization algorithm.

3.2. Calibration setup and execution

A stochastic optimization method, namely DES (Derandomized Evolution Strategy), was chosen for the calibration process. As a matter of fact, due to the strong nonlinearity of the specific optimization problem,

Table 1
Parameters range for DOE and optimization processes.

Variable	DOE range	Optimization range
$\overline{f}_{AF}$	[0.001, 0.01]	[10^{-6}, 1]
f_{AV}	[0.001, 0.01]	[10^{-6}, 1]
$\beta_{trap,open}$	[1, 40]	[0.1, 150]
$\beta_{trap,shut}$	[10^3, 10^4]	[500, 15,000]
β_{vent}	[1, 40]	[0.1, 150]
f_{tunnel}	[0.01, 0.05]	[0.001, 0.1]

Table 2
Calibrated parameter set (left), RMS deviation for each of the 5 cases (right).

Parameter	Value
f_{AF-1F}	1.93 $\times 10^{-2}$
f_{AF-2F}	9.42 $\times 10^{-3}$
f_{AF-3F}	1.50 $\times 10^{-3}$
f_{AF-4F}	1.29 $\times 10^{-1}$
f_{AF-1I}	4.67 $\times 10^{-5}$
f_{AF-2I}	4.96 $\times 10^{-3}$
f_{AF-3I}	1.42 $\times 10^{-2}$
f_{AF-4I}	1.90 $\times 10^{-2}$
f_{AV}	3.97 $\times 10^{-2}$
$\beta_{trap,open}$	13.3
$\beta_{trap,shut}$	1.96 $\times 10^3$
β_{vent}	72.6
f_{tunnel}	2.55 $\times 10^{-2}$
Case id	RMS deviation [m/s]
1	0.21
2	0.32
3	0.17
4	0.30
5	0.31

which is likely to show a number of local minimum points, deterministic methods would prove unsuitable for the task. A more detailed explanation of the optimization algorithm can be found in [22] and is omitted here for the sake of brevity.

The objective function is the sum of square deviations between calculated and measured velocity values, evaluated on 1115 points uniformly spread along the main tunnel, for all the five experimental cases. The aim of the optimization process is, obviously, to find a global minimum of the objective function.

As the experimental data refer to the five different acquisitions presented in [1] the test suite has been set up that, given a set of values of 13 parameters, five subsequent calculations are run, and their error function are evaluated and summed to represent an overall error value. The calibration process is then carried out as an optimization aimed at finding the set of parameters which minimizes such value.

The initial population size has been set to 120 individuals. A Latin Hypercube Design of Experiments (DOE) [23] has been adopted to generate the initial population.

The design space, represented by the ranges of variability of each calibration parameter, is reported in Table 1. The ranges chosen for the generation of the initial population have been extended for the optimization process to allow a wider exploration.

It is worth to mention that at each generation step, within the optimization process, the most computationally demanding part is the evaluation of the fitness of the individuals. Such evaluations are independent from each other, thus a parallel implementation of the process led to notable savings in terms of computational time.

The calibration process has taken 2500 generations of 120 individuals each, for a total of 300,000 evaluations of the error function. Each evaluation required five simulation runs.

4. Results

The best fit of the parameter set, as determined by the optimization algorithm is reported in Table 2. RMS deviations from experimental data, for each of the five simulations associated to the experimental tests, are added to the table. Some observations on the obtained parameter values are in order. Concerning the nine friction factors (8 for each of the AF channels and one for the AV channels), most of the computed values lie in the range 10^{-2} to 4×10^{-2}: this is in line with typical values used in road tunnel ventilation models [18]. However, some of the values appear as unusually much lower or higher with respect to this range. For instance, the obtained value for AF-4F is of order 10^{-1}: this could be ascribed to the presence of flush-mounted wireways hosting network communication backbones and electric connections. The value is significantly higher with respect to the corresponding channel on the Italian side (AF-4I), and this could be explained by the different shapes of the two channels (the AF-4F channel is barrel-vaulted with a smaller cross-section, while the AF-4I channel is substantially rectangular), thus implying a different impact of the flush-mounted elements on the computed overall friction factor.

On the opposite end, a value of order 5×10^{-5} for the AF-1I channel can appear, at a first glance, as non-physical for a concrete duct. The obtainment of such a low value might be justified by different, concurrent factors. First, the choice of a unique concentrated loss coefficient β_{vent}

for all the 1161 fresh air vents implies a certain degree of compensation between this value and the friction factors of the individual ducts. As a matter of fact, since fresh air discharge is performed all along the tunnel (see [1]), mechanical energy losses occurring between fresh air fans and tunnel openings are the sum of friction losses in both channels and vents. To this regard, it has to be mentioned that both AF-1 channels are shorter, and are connected with the tunnel through fresh air vents along their entire length, while all the other AF channels are divided into a *transfer* stretch (where the flow rate is constant, since no vents are present) and a *distribution* stretch (along which fresh air is discharged in the tunnel through vents). For this reason, in the case of the AF-1I channel, the obtained value of β_{vent} might account for almost all of the friction losses, thus leading to the determination of an extremely low value of the f_{AF-1I} factor. The same consideration can explain also the values of f_{AF-2I} and f_{AF-3F}, which are slightly below the aforementioned range of typical f-values. Moreover, it is worthy to point out that velocity measurements close to the Italian portal (corresponding to the tunnel stretch served by the AF-1I channel) have been found to be affected by a greater degree of noise: such an occurrence is undoubtedly expected to affect the result of the calibration process, and, thus, the obtained value of f_{AF-1I}. Nevertheless, the computed value for the corresponding AF-1F channel is more in line with expectations, but it has to be mentioned that, by visual inspection, such a channel was found to be particularly obstructed by obstacles of various kinds, which certainly do not facilitate the flow of air in what is an already very narrow duct.

Finally, the tunnel friction factor f_{tunnel} as estimated by the optimization process is consistent with the result obtained in a previous calibration of a 0D model [4]. In fact, the calibrated value, $f = 0.0255$, differs by less than 8% from the result of the previous study, $f = 0.0235$, thus corroborating the validity of the chosen modeling and calibration approach.

Fig. 2 shows the longitudinal air velocity profile, as predicted by the calibrated model, for each of the five benchmark cases considered, alongside with the velocity profiles measured by the T.A.L.P.A. facility (see part I of the present work, [1]). Velocity data simultaneously measured by the fixed anemometers permanently installed in the tunnel are also added to the graphs for further reference.

The model response to the calibration process can be viewed as satisfactory, according to the results reported in Fig. 2. Although slight differences between calculated and measured profiles can be observed, especially for the cases where the extraction system was turned on (tests 2, 4 and 5, see [1]), the overall profile shape and slope changes are captured accurately.
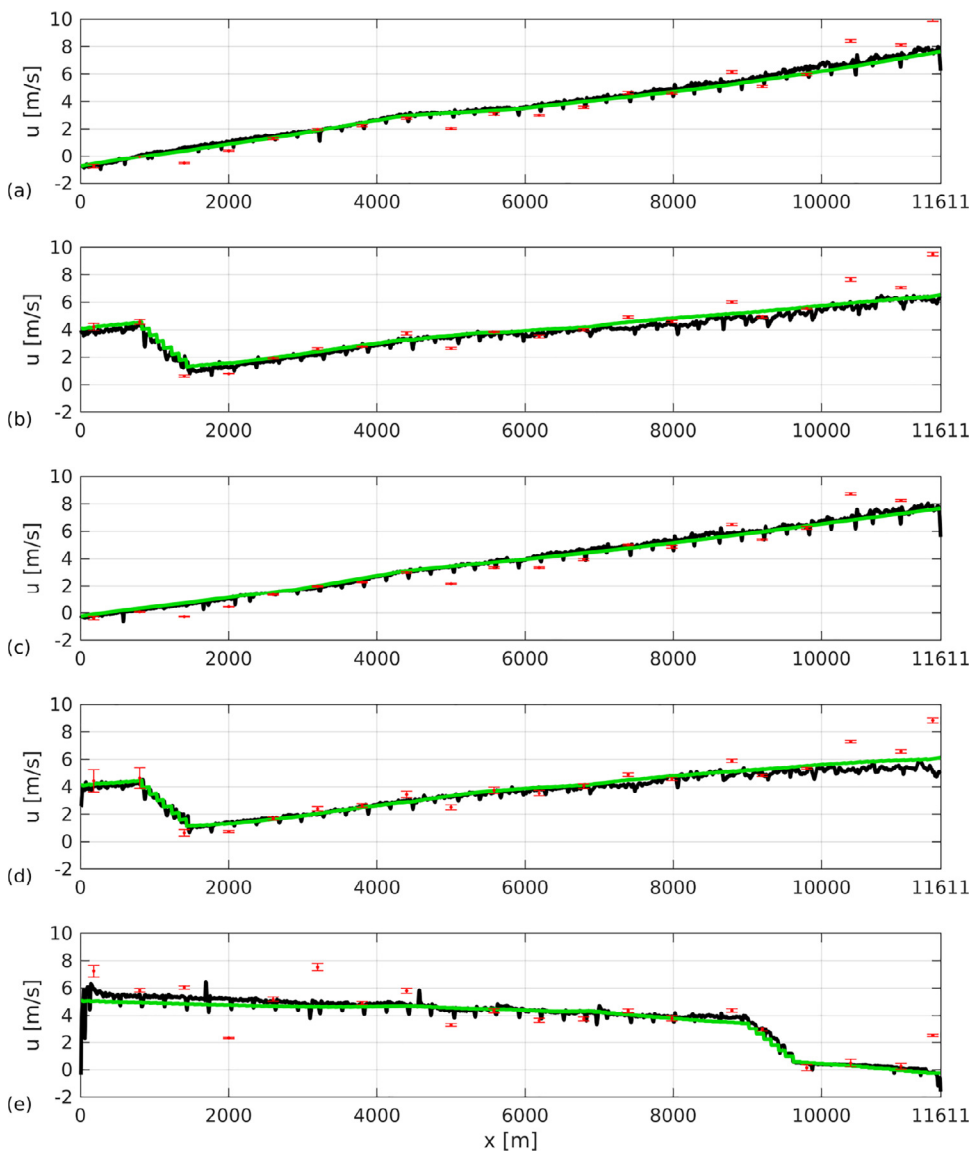
Fig. 2. Comparison between calculated velocity profile (green), measured velocity profile (black) and velocity measurements taken by the tunnel anemometers (red) for all of the five benchmark tests described in [1]: (a) Test n. 1, (b) Test n. 2, (c) Test n. 3, (d) Test n. 4, (e) Test n. 5.

As already touched on previously, measurements close to the Italian exit ($x = 11611$) are affected by a higher noise: this can be also evinced by the significant deviation that can be observed between present experimental data and the values given by the TMB fixed-point anemometers. Unsurprisingly, the highest deviation between numerical results and benchmark measurement data also generally occurs in that region.

The numerical results obtained on the benchmark calibration cases are surely encouraging, but do not prove thoroughly the reliability of the model on the full spectrum of working conditions which can take place in the physical tunnel. An extra pool of data, *unknown* to the model, is required for a proper model validation. The tunnel control system keeps a record of the flow and boundary conditions, as measured during emergency events or extraction system trial runs: such data constitutes an ideal choice for full model validation.

To the extent of the present study, the comparison has been performed only between steady-state numerical simulations and velocity measurements taken from the Mont Blanc Tunnel database, collected at selected dates and times.

As it can be observed in Fig. 3, the numerical model provides a satisfactory approximation if the calculated velocity profile is compared to the local values measured by the tunnel anemometers. Comparing then the output of the numerical model with the velocity profile as calcu-

lated by the tunnel control system *SCADA* (which uses the flow rates measured in the ventilation ducts for obtaining the profile shape, and then fits the profile based on the values collected by the anemometers), although small local deviations are present, the overall trend is always successfully captured.

5. Concluding remarks

In the present work, Part II of a twofold study, a numerical procedure for the calculation of airflow in a road tunnel ventilation system was presented and applied to the case of the Mont Blanc Tunnel. The method is based on a Finite Volume discretization of mass, mechanical energy and thermal energy conservation equations, under the hypothesis of 1D, steady-state flow. The topology of the network of ducts that constitute the ventilation system is represented by means of an oriented graph. The numerical resolution of the discretized equations is based on a modified version of the SIMPLE algorithm. The method was described in detail, highlighting the peculiar strategies adopted to treat source and sink terms, and variable transfer from nodes to branches of the network and vice-versa.

Successively, a model network of the Mont Blanc Tunnel ventilation system was constructed, representing the tunnel itself and its fresh air intake and exhaust air extraction channels, with a spatial resolution as
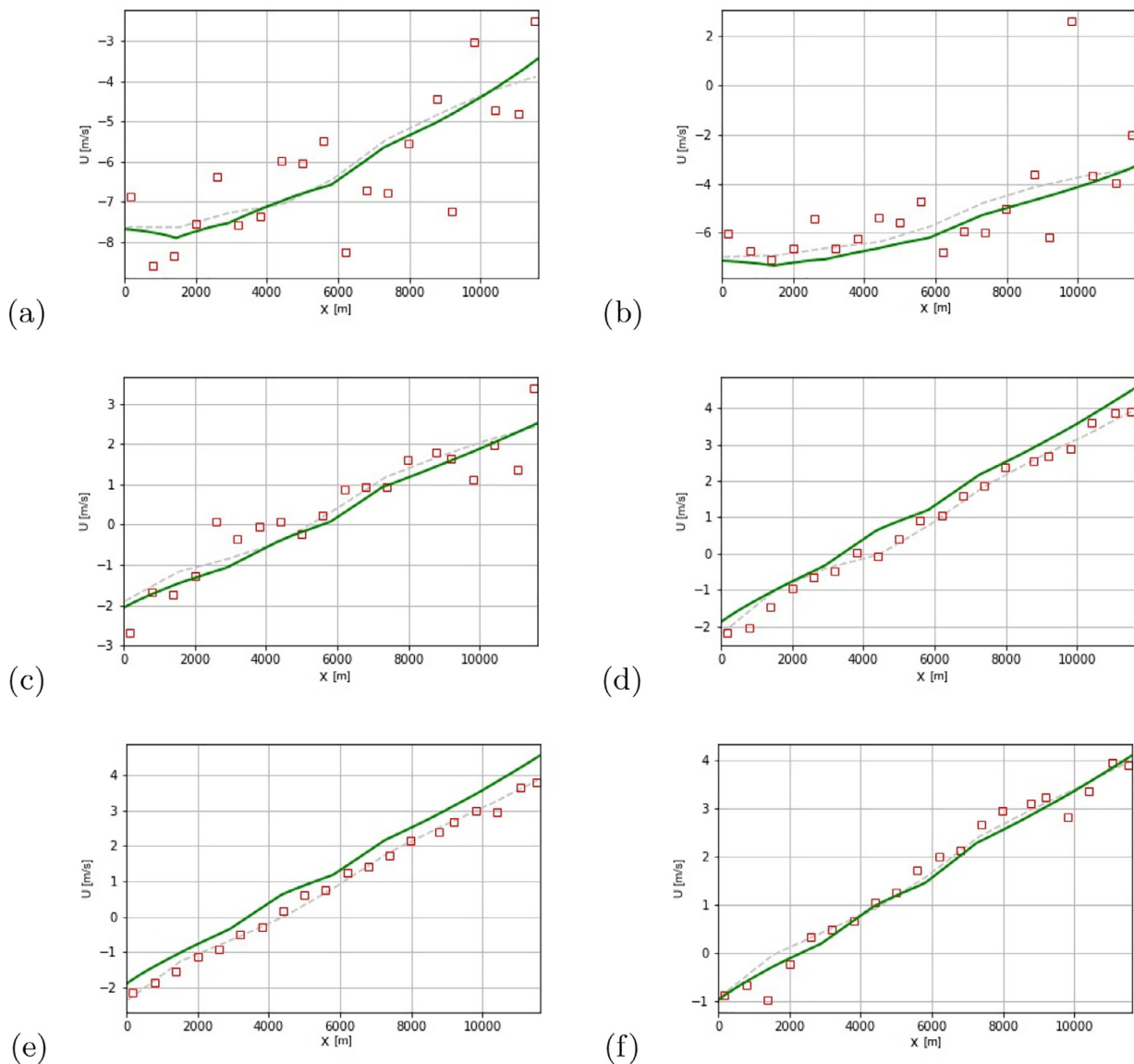
Fig. 3. Validation of the algorithm against experimental data provided from the fixed sensors installed in the tunnel, on different occasions. Green line: calculated velocity profile. Gray dotted line: velocity profile as calculated by the tunnel control system (SCADA). Red squares: local velocity as measured by fixed anemometers. (a) 2018-03-01 03:37:00, $\Delta p = -850.59$ Pa (b) 2018-03-01 06:12:41, $\Delta p = -746.49$ Pa (c) 2018-10-07 14:15:30, $\Delta p = 29.59$ Pa (d) 2019-04-09 05:40:45, $\Delta p = 117.21$ Pa (e) 2019-05-16 16:13:46, $\Delta p = 116.69$ Pa (f) 2019-05-27 23:29:27, $\Delta p = 117.46$ Pa.

small as 10 m. A set of 13 parameters representing friction losses within the various parts of the system was defined; parameter values were then calibrated against an experimental benchmark dataset of longitudinal velocity profiles, measured along the tunnel by means of a custom-made survey rake during five in situ tests performed at the Mont Blanc Tunnel. These data, along with the experimental facility, were presented in Part I of this study.

Calibration of the parameter set was performed by mean of genetic optimization algorithm, namely DES (Derandomized Evolution Strategy). With the optimized parameter values, a good agreement between the predicted velocity profiles and the experimental data was found, with an overall RMS deviation of ± 0.27 m/s, lower than the measurement accuracy of the probes used for the experimental campaign. Given the complexity of the model, and the relatively low number of loss coefficients chosen for calibration, the obtained accuracy has to be regarded as highly satisfactory. The method was then successfully validated against further data coming from field measurements taken by the fixed anemometers installed in the Mont Blanc Tunnel control system.

Together with the experimental facility described in the first part of the study, the presented approach stands as a one-of-a-kind, robust methodology for analyzing, modeling and predicting airflow in road tunnel ventilation systems. The methodology could be applied with acceptable effort to any tunnel, and, with suitable adaptations of the experimental facility, also to different kinds of infrastructures that could be modeled as a network of ducts.

Declaration of Competing Interest

The authors declare that they have no known competing financial interests or personal relationships that could have appeared to influence the work reported in this paper.

The authors declare the following financial interests/personal relationships which may be considered as potential competing interests:

References

[1] P. Levoni, D. Angeli, P. Cingi, G. Barozzi, M. Cipollone, An integrated approach for

the analysis and modeling of road tunnel ventilation. Part I: Continuous measurement of the longitudinal airflow profile, Transp. Eng. 3 (2021) 100039.

[2] P. Levoni, D. Angeli, E. Stalio, G. Barozzi, M. Cipollone, Concept, design, construction and testing of an experimental facility for multi-point longitudinal air flow measurements in tunnels, in: Proceedings of the 29th UIT Heat Transfer Conference, 2011, pp. 507–512.

[3] P. Levoni, A. Scorcioni, D. Angeli, E. Stalio, G. Barozzi, M. Cipollone, TALPA: an innovative facility for continuous longitudinal airflow profile acquisition in tunnels, in: Proceedings of the 30th UIT Heat Transfer Conference, 2012, pp. 325–330.

[4] P. Levoni, D. Angeli, E. Stalio, E. Agnani, G. Barozzi, M. Cipollone, Fluid-dynamic characterisation of the Mont Blanc Tunnel by multi-point airflow measurements, Tunn. Undergr. Space Technol. 48 (2015) 110–122.

[5] E. Agnani, D. Angeli, I. Spisso, P. Levoni, E. Stalio, G. Barozzi, M. Cipollone, Full scale CFD modeling of the Mont Blanc Tunnel ventilation system, in: Proceedings of the 31st UIT Heat Transfer Conference, 2013, pp. 349–358.

[6] R.E. Greuer, Study of Mine Fires and Mine Ventilation: Part I, Computer Simulation of Ventilation Systems Under the Influence of Mine Fires, Michigan, 1977.

[7] R. Schlaug, Users Guide for the TUNVEN and DUCT Programs, Technical Report, Science Applications, Inc., La Jolla (CA), USA, 1980.

[8] I. Riess, M. Bettelini, R. Brandt, Sprint-a design tool for fire ventilation, in: Proceedings of the BHR Group Conference Series Publication, 43, Bury St. Edmunds; Professional Engineering Publishing; 1998, 2000, pp. 629–638.

[9] A. Majumdar, J. Bailey, B. Sarkar, A. Majumdar, J. Bailey, B. Sarkar, A generalized fluid system simulation program to model flow distribution in fluid networks, in: Proceedings of the 33rd Joint Propulsion Conference and Exhibit, 1997, p. 3225.

[10] M.C. Weng, L.X. Yu, F. Liu, P.V. Nielsen, Full-scale experiment and CFD simulation on smoke movement and smoke control in a metro tunnel with one opening portal, Tunn. Undergr. Space Technol. 42 (2014) 96–104.

[11] A. Król, M. Król, Transient analyses and energy balance of air flow in road tunnels, Energies 11 (7) (2018).

[12] P. Reszka, T. Steinhaus, H. Biteau, R. Carvel, G. Rein, J.L. Torero, A study of fire durability for a road tunnel: comparing CFD and simple analytical models, in: J. Eberhardsteiner (Ed.), Proceedings of the ECCOMAS Thematic Conference on Computational Methods in Tunnelling (EURO:TUN 2007), 2008.

[13] F. Colella, G. Rein, R. Borchiellini, R. Carvel, J.L. Torero, V. Verda, Calculation and design of tunnel ventilation systems using a two-scale modelling approach, Build. Environ. 44 (12) (2009) 2357–2367.

[14] F. Colella, G. Rein, R. Carvel, P. Reszka, J.L. Torero, Analysis of the ventilation systems in the Dartford tunnels using a multi-scale modelling approach, Tunn. Undergr. Space Technol. 25 (4) (2010) 423–432.

[15] F. Colella, G. Rein, R. Borchiellini, J.L. Torero, A novel multiscale methodology for simulating tunnel ventilation flows during fires, Fire Technol. 47 (1) (2011) 221–253.

[16] I. Vermesi, G. Rein, F. Colella, M. Valkvist, G. Jomaas, Reducing the computational requirements for simulating tunnel fires by combining multiscale modelling and multiple processor calculation, Tunn. Undergr. Space Technol. 64 (2017) 146–153.

[17] A. Król, M. Król, P. Koper, P. Wrona, Numerical modeling of air velocity distribution in a road tunnel with a longitudinal ventilation system, Tunn. Undergr. Space Technol. 91 (2019).

[18] H.-M. Jang, F. Chen, On the determination of the aerodynamic coefficients of highway tunnels, J. Wind Eng. Ind. Aerodyn. 90 (8) (2002) 869–896.

[19] R. Diestel, Graph Theory, Springer, 1997.

[20] S.V. Patankar, Numerical Heat Transfer and Fluid Flow, Hemisphere Publishing Corporation (CRC Press, Taylor & Francis Group), 1980.

[21] V. Ferro, R. Borchiellini, V. Giaretto, Description and application of tunnel simulation model, in: Proceedings of the Aerodynamics and Ventilation of Vehicle Tunnels Conference, 1991, pp. 487–512.

[22] P. Cingi, D. Angeli, M. Cavazzuti, P. Levoni, M. Cipollone, Development and calibration of a 1D thermo-fluid dynamic model of ventilation in tunnels, J. Phys.: Conf. Ser. 1599 (1) (2020). art. no. 012048

[23] M. Cavazzuti, Optimization Methods: From Theory to Design, Springer, 2015.